

PHILOSOPHICAL TRANSACTIONS OF THE ROYAL SOCIETY B

BIOLOGICAL SCIENCES

Recombination landscape dimorphism contributes to sex chromosome evolution in the dioecious plant *Rumex hastatulus*

| | |
|---|--|
| Journal: | <i>Philosophical Transactions B</i> |
| Manuscript ID | Draft |
| Article Type: | Research |
| Date Submitted by the Author: | n/a |
| Complete List of Authors: | Rifkin, Joanna; Univ of Toronto, Ecology & Evolutionary Biology Hnatovska, Solomiya; Univ of Toronto, Ecology & Evolutionary Biology Yuan, Meng; Univ of Toronto, Ecology & Evolutionary Biology Sacchi, Bianca; Univ of Toronto, Ecology & Evolutionary Biology Choudhury, Baharul; Queen's University Gong, Yunchen; Univ of Toronto, Ecology & Evolutionary Biology Rastas, Pasi; University of Helsinki, Institute of Biotechnology Barrett, Spencer; Univ of Toronto, Ecology & Evolutionary Biology; Wright, Stephen; University of Toronto, |
| Issue Code (this should have already been entered and appear below the blue box, but please contact the Editorial Office if it is not present): | SEXPLANTS |
| Subject: | Evolution < BIOLOGY, Genetics < BIOLOGY, Plant Science < BIOLOGY, Genomics < BIOLOGY |
| Keywords: | dioecy, evolution, gametophytic competition, heterochiasmy, recombination, sex chromosomes |
| | |

SCHOLARONE™
Manuscripts

bioRxiv preprint doi: <https://doi.org/10.1101/2021.11.03.466946>; this version posted November 4, 2021. The copyright holder for this preprint (which was not certified by peer review) is the author/funder, who has granted bioRxiv a license to display the preprint in perpetuity. It is made available under a [CC-BY-NC-ND 4.0 International license](#).

Author-supplied statements

Relevant information will appear here if provided.

Ethics

Does your article include research that required ethical approval or permits?:

This article does not present research with ethical considerations

Statement (if applicable):

CUST_IF_YES_ETHICS :No data available.

Data

It is a condition of publication that data, code and materials supporting your paper are made publicly available. Does your paper present new data?:

Yes

Statement (if applicable):

CUST_IF_YES_DATA :No data available.

Conflict of interest

I/We declare we have no competing interests

Statement (if applicable):

CUST_STATE_CONFLICT :No data available.

Authors' contributions

This paper has multiple authors and our individual contributions were as below

Statement (if applicable):

Joanna L. Rifkin coordinated and performed descriptive genomics analyses and linear models and participated in conceiving and writing the paper

Solomiya Hnatovska performed the TE annotation

Meng Yuan performed differential expression analyses

Bianca Sacchi performed differential expression analyses and SNP-calling

Baharul Choudhury coordinated plant growth and nucleic acid expression

Yunchen Gong created the transcriptome annotation

Pasi Rastas generated the linkage maps and the improved genome assembly

Spencer C.H. Barrett provided funding, development, and editing

Stephen I. Wright conceived, funded, coordinated, and coauthored the paper

bioRxiv preprint doi: <https://doi.org/10.1101/2021.11.03.466946>; this version posted November 4, 2021. The copyright holder for this preprint (which was not certified by peer review) is the author/funder, who has granted bioRxiv a license to display the preprint in perpetuity. It is made available under a [CC-BY-NC-ND 4.0 International license](#).

Recombination landscape dimorphism contributes to sex chromosome evolution in the dioecious plant

Rumex hastatulus

Joanna L. Rifkin^{1*}, Solomiya Hnatovska¹, Meng Yuan¹, Bianca M. Sacchi¹,
Baharul I. Choudhury^{1,2}, Yunchen Gong³, Pasi Rastas⁴, Spencer C.H. Barrett¹,
Stephen I. Wright^{1,3*}

1 – Department of Ecology and Evolutionary Biology, University of Toronto, Toronto, ON
Canada

2 – Department of Biology, Queen's University, Kingston, ON, Canada

3 – Centre for Analysis of Genome Evolution and Function, University of Toronto, Toronto, ON
Canada

4 – Institute of Biotechnology, University of Helsinki, Finland

Keywords: dioecy, evolution, gametophytic competition, heterochiasmy,
recombination, sex chromosomes

1
2
3
4
5
6
7
8
9
10
11
12
13
14
15
16
17
18
19
20
21
22
23
24
25
26
27
28
29
30
31
32
33
34
35
36
37
38
39
40
41
42
43
44
45
46
47
48
49
50
51
52
53
54
55
56
57
58
59
60

bioRxiv preprint doi: <https://doi.org/10.1101/2021.11.03.466946>; this version posted November 4, 2021. The copyright holder for this preprint (which was not certified by peer review) is the author/funder, who has granted bioRxiv a license to display the preprint in perpetuity. It is made available under a [CC-BY-NC-ND 4.0 International license](#).

*Corresponding authors' contact information: joanna.rifkin@utoronto.ca, joannarifkin@gmail.com, stephen.wright@utoronto.ca

For Review Only

1 Summary

2 There is growing evidence across diverse taxa for sex differences in the genomic landscape of
3 recombination, but the causes and consequences of these differences remain poorly understood. Strong
4 recombination landscape dimorphism between the sexes could have important implications for the
5 dynamics of sex chromosome evolution and turnover because low recombination in the heterogametic
6 sex can help favour the spread of sexually antagonistic alleles. Here, we present a sex-specific linkage
7 map and revised genome assembly of *Rumex hastatulus*, representing the first characterization of sex
8 differences in recombination landscape in a dioecious plant. We provide evidence for strong sex
9 differences in recombination, with pericentromeric regions of highly suppressed recombination in males
10 that cover over half of the genome. These differences are found on autosomes as well as sex
11 chromosomes, suggesting that pre-existing differences in recombination may have contributed to sex
12 chromosome formation and divergence. Analysis of segregation distortion suggests that haploid
13 selection due to pollen competition occurs disproportionately in regions with low male recombination.
14 Our results are consistent with the hypothesis that sex differences in the recombination landscape
15 contributed to the formation of a large heteromorphic pair of sex chromosomes, and that pollen
16 competition is an important determinant of recombination dimorphism.

18 Introduction

19 The distribution of rates of recombination along chromosomes (recombination landscape [1]) shapes
20 many aspects of evolutionary genetics, including the efficacy of natural selection [2], genome structure
21 [3], and the dynamics of reproductive isolation [4]. Rates of recombination can vary between species,
22 between and within chromosomes, and between male and female meiosis in both
23 dioecious/gonochoristic and hermaphroditic species [5–7]. We refer to this phenomenon as ‘sex
24 differences in the recombination landscape’ [1]. Although sex differences in the rate and distribution of
25 recombination appear to be widespread and variable, the causes and consequences of this variation
26 have only recently been investigated in detail [1,6,8].

27
28 Many components of evolutionary processes depend on the sex-averaged rate of recombination.
29 Nevertheless, sex differences in recombination (heterochiasmy) in dioecious populations can have
30 important consequences for the evolution of sex chromosomes. This is because on the sex chromosome

1
2
3 31 restricted to the heterogametic sex (i.e. the Y or W chromosome), sex-specific recombination landscapes
4 32 entirely control the rate of recombination, and thereby influence the scale of recombination
5 33 suppression surrounding a sex-determining region (SDR) [1]. Recently, heterochiasmy has been
6 34 proposed as an important factor in maintaining sexually antagonistic (SA) variants on the sex
7 35 chromosomes even in the absence of recombination modifiers [9]. In particular, SA alleles can spread
8 36 more easily through populations because of pre-existing male-specific suppression of recombination,
9 37 rather than recombination suppression evolving as a secondary consequence of the segregation of SA
10 38 alleles [9]. Variation among species in patterns of heterochiasmy could thus be an important general
11 39 determinant of the evolution of sex chromosomes and their turnover [1], potentially contributing to
12 40 differences among lineages in the likelihood of the formation of heteromorphic sex chromosomes, the
13 41 maintenance of sexually antagonistic polymorphisms and the size of the SDR.
14
15
16
17
18
19
20
21
22

23 43 Several patterns are evident in the characteristics of sexual dimorphism in the recombination landscape.
24 44 First, although data are limited, many eukaryotes have recombination rates biased towards the tips of
25 45 chromosomes in male meiosis, whereas female recombination rates are more likely to be either
26 46 elevated towards the centromeres or are more uniform across the chromosome [1]. In hermaphroditic
27 47 plants, three of five taxa studied show this pattern [10–12], although in maize there was limited
28 48 evidence for large-scale differences in recombination between male and female meiosis [13], and in an
29 49 interspecific cross between *Solanum esculentum* and *S. pennellii* recombination in male gametes was
30 50 reduced genome-wide compared with female gametes [14]. Preliminary analysis of genetic maps in the
31 51 dioecious *Mercurialis annua* do not suggest major sex differences in recombination rates [15], although
32 52 the genomic context of these maps is still being investigated. In general, however, recombination rate
33 53 landscape dimorphism has not yet been investigated in dioecious plants, limiting our understanding of
34 54 its potential role in the evolutionary dynamics of plant sex chromosomes.
35
36
37
38
39
40
41
42
43
44

45 56 Many species have convergently evolved tip-biased recombination in male meiosis [1], but the reasons
46 57 for this pattern are unclear. Both non-adaptive and adaptive explanations have been proposed. If
47 58 recombination landscape differences are not adaptive, they may simply result from mechanistic
48 59 differences between the process of female and male meiosis [1]. Adaptive hypotheses include sexually
49 60 antagonistic selection favoring tighter linkage between sex-specific genes and regulatory elements [1],
50 61 selection favoring recombination near the centromere in female meiosis to remove meiotic drive alleles
51 62 [7], and epistatic haploid selection on male gametes and gametophytes [6]. In plants, evidence that

63 female recombination rates are elevated relative to male recombination rates in outcrossing species
64 compared with selfing species [6] is consistent with models of both female meiotic drive and male
65 gametophytic selection, as both are expected to be more intense with higher rates of outcrossing [6,7].
66 Disentangling these alternatives is challenging and will require more comparative information on sex-
67 specific recombination in both hermaphroditic and dioecious taxa.

68
69 *Rumex hastatulus* is a dioecious, wind-pollinated plant with heteromorphic sex chromosomes [16,17].
70 Recent genome sequencing combined with high marker-density linkage mapping has revealed that the
71 SDR is embedded within a very large genomic region of highly suppressed recombination [18]. Evidence
72 for similarly large non-recombining regions in the pericentromeric regions of autosomes suggested that
73 pre-existing recombination suppression may have contributed to the formation of large heteromorphic
74 sex chromosomes in *R. hastatulus* [18]. However, this study measured sex-averaged recombination
75 rates, limiting our ability to investigate the potential role of heterochiasmy in sex chromosome
76 formation and maintenance. With earlier evidence for an important role for gametophytic selection on
77 the sex ratio in this species [19,20], the influence of pollen competition in the evolution of the sex
78 chromosomes [21], and indications of frequent male and female transmission distortion in related
79 dioecious *Rumex* taxa [22], there is a strong likelihood that haploid selection in males and/or females
80 may contribute to sex-specific selection favouring sexual dimorphism in recombination landscapes in
81 this system.

82
83 Here, we explore the potential importance of heterochiasmy for the evolution of sex chromosomes and
84 test hypotheses concerning the evolutionary forces favouring sex-specific recombination rate
85 differences in *R. hastatulus*. Using a sex-specific linkage map and corrected draft genome assembly, we
86 first determine whether *R. hastatulus* shows evidence for heterochiasmy and other sex differences in
87 recombination landscape and compare this pattern between the sex chromosome and the autosomes.
88 We then examine the correlates of male and female recombination rates genome-wide and use this
89 information to explore the potential role of sexual antagonism, haploid selection, and meiotic drive as
90 evolutionary drivers of sexual dimorphism in the recombination landscape.

91

92 Methods

93 Linkage mapping and genome assembly

94 We generated a mapping population from a cross between a male and female derived from a single
95 population collected in Rosebud, TX [20]. Seeds from the field collection were grown in the glasshouse
96 and at onset of flowering one male and one female individual were randomly paired for a controlled
97 cross to develop the F₁ generation. Paired plants were immediately moved into miniature crossing
98 chambers [23] to avoid pollen contamination from other plants growing in the same glasshouse, and F₁
99 seeds were harvested after maturation. To obtain tissue from F₁ plants, we sterilized seeds using 5%
100 (V/V) bleach and germinated them on filter paper in refrigerated petri dishes. After germination, we
101 transplanted seedlings into six-inch plastic pots containing a 3:1 ratio of Promix soil and sand and a slow-
102 release fertilizer (Nutricote, 14:13:13, 300mL per 60lbs) and placed them in a glasshouse at the
103 University of Toronto, St. George campus. We watered plants every other day, and their positions on
104 benches were randomized weekly. On day 43 or 44 after transplant, between 10:00 and 12:00, we
105 collected and flash-froze 30mg of leaf tissue for RNA extraction using liquid nitrogen. When plants
106 flowered, we phenotyped for sex. We used Spectrum Plant Total RNA Kits (Sigma Aldrich) for RNA
107 extraction. The sequenced library included 188 individuals: 102 female offspring, 84 male offspring, and
108 three replicate samples of each parent.

109
110 For library preparation and sequencing, we sent our RNA samples to the Centre d'expertise et de
111 services Génome Québec (CES, McGill University, Montréal, QC, Canada). CES prepared libraries using
112 NEBNext library prep kits and sequenced them on a NovaSeq6000 S4 PE100. Sequencing resulted in a
113 total of 3.1 billion reads (3,060,570,370), with between 10 and 49 million reads per sample (mean
114 15,940,471, median 14,548,490). Raw sequence has been deposited on the Sequence Read Archive
115 (SRA) under the accession number PRJNA692236 (embargoed until July 1, 2022 or publication).

116
117 We aligned our raw sequencing reads to the *R. hastatulus* Dovetail draft genome assembly [18] using
118 Star 2-pass version 2.7.6 [24,25]. We processed the aligned files to sort, mark PCR duplicates, and
119 (splitNCigar reads) using PicardTools (<http://broadinstitute.github.io/picard/>) and the Genome Analysis
120 Tool Kit [26].

1
2
3 121 We initially generated a linkage map using Lep-Map3 [27] from reads aligned to the original *R.*
4
5 122 *hastatulus* draft assembly. The markers could be split into five linkage groups using a LOD score limit of
6
7 123 30 for the initial split followed by a LOD score limit of 34 for the resulting largest linkage group
8
9 124 (SeparateChromosomes2). Most of the remaining single markers were put into these groups using a LOD
10
11 125 score limit of 25 (JoinSingles2All), totaling about 120,000 markers. We then calculated the marker order
12
126 for each linkage group with OrderMarkers2 (with default settings).

13
14
15 128 To improve our linkage map, we reduced redundancy in our genome assembly and constructed a new
16
17 129 pseudo-chromosome assembly using the Lep-Anchor [28] software. To obtain reliable linkage maps, we
18
19 130 removed the 13 most-recombining individuals from the maps and constructed three independent
20
21 131 linkage maps (Lep-MAP3: OrderMarkers2), using only male informative markers (parameter
22
23 132 informativeMask=1), only female informative markers (informativeMask=2) and all markers. These maps
24
25 133 were used by the Lep-Anchor software.

26
27 135 To reduce redundancy in the genome assembly, we first split the existing Dovetail assembly into contigs
28
29 136 based on assembly gaps. Due to a high number of contigs (>44,000), we removed all contigs of < 500bp,
30
31 137 full length haplotypes and joined partial haplotypes in windows of five adjacent contigs (link strength
32
33 138 was $6 - |\text{distance}| - |\text{difference in orientations}|$, where distance between contig *i* and *j* is $|i-j|$ and
34
35 139 difference is 0-2 based on how the orientations differ: same=0, one different=1, both different=2). This
36
37 140 was done by Lep-Anchor giving it only the alignment chain computed by Haplomerger2 [29] on the
38
39 141 WindowMasker [30] soft-masked (contig-split) genome. This allowed us to reduce the number of contigs
40
41 142 to about 33,000. All data were lifted to the new contig assembly coordinates using the liftover script and
42
43 143 LiftoverHaplotypes module in Lep-Anchor.

44
45 145 We then ran Lep-Anchor (lepanchor_wrapper2.sh) on the final contig assembly using the three linkage
46
47 146 maps, new alignment chains (HaploMerger2) and alignments of raw Pacbio sequence aligned by
48
49 147 minimap2 [31]. The resulting pseudo-chromosome assembly was used to calculate physical order of
50
51 148 linkage map markers and the maps were evaluated (OrderMarkers2 parameter evaluateOrder) in this
52
53 149 order to obtain the final linkage maps. After assembly improvement, we compared contig orders
54
55 150 between our previous [18] and new maps using custom R scripts incorporating Plotly [32] interactive
56
57 151 plotting.

152 **Recombination rates and transmission distortion**

153 We quantified recombination rates in two ways. First, we described recombination using map lengths in
154 centimorgans (cM) from the maps produced by Lep-Map3. Based on the scale of recombination
155 observed in previous work [18] and the current map, we performed all downstream analyses using 1Mb
156 windows. We also calculated recombination rates as the sum of crossover events per 1Mb window. We
157 first calculated the number of crossovers per site from cM differences using the inverse of the Haldane
158 mapping function [33], then summed crossovers in 1Mb windows. To describe the extent of
159 recombination suppression, we identified the total number of consecutive windows with zero
160 crossovers. We estimated transmission ratio distortion as a likelihood ratio of the deviation from 1:1
161 transmission of haplotypes from the male and female parent using custom scripts by PR.

163 **Gene and TE content**

164 We also developed a new annotation using MAKER version 3.01.03 [34]. For our MAKER annotation, we
165 used the soft-masked [30] genome integrated with previously published floral transcriptomes from six
166 individuals [21] and leaf transcriptomes from six populations [17]. Transcripts were assembled with
167 IDBA-tran version 1.2.0 [35] and annotated in four rounds, using the transcripts and the Tartary
168 buckwheat annotation version FtChromosomeV2.IGDBv2 [36] as the evidences for MAKER. We
169 functionally annotated the final annotation based on homology using BLAST version 2.2.28+ [37] and
170 InterProScan 5.52-86.0 [38]. This annotation resulted in 59,121 genes. We also annotated the locations
171 of rDNA repeats using rnammer-1.2 [39]. The parameters used, '-S euk' and '-m tsu,ssu,lsu', indicate that
172 the input reference is a eukaryote, and that we are annotating 5/8s, 16/18s, and 23/28s rDNA.

174 We produced the TE annotation using the EDTA (Extensive de-novo TE Annotator) version 1.9.7 pipeline
175 [40]. This pipeline combines the best-performing structure- and homology-based TE finding programs
176 (LTR_FINDER_parallel [41], LTR_HARVEST_parallel [42], LTR_retriever [43], TIR-Learner2.5 [44],
177 HelitronScannerv1.1[45], Repeatmodeler-2.0.1 [46] and RepeatMasker-4.1.1 [47] and filters their results
178 to produce a comprehensive and non-redundant TE library [40]. The optional parameters '--sensitive 1'
179 and '--anno 1' were used to identify remaining unidentified TEs with RepeatModeler and to produce an
180 annotation. The 'EDTA.TEanno.split.gff3' output file was used as our non-overlapping TE annotation. This
181 file is produced by EDTA by removing overlaps according to the following priorities: structure-based

182 annotation > homology-based annotation, longer TE > shorter TE > nested inner TE > nested outer TE
183 [40].

184
185 For all gene content analyses, we used a stringently filtered set of genes to remove gene annotations
186 associated with transposable elements. We first used BEDtools [48] to remove any exons that
187 overlapped a TE, although genes containing both exons that overlapped TEs and exons that did not
188 overlap TEs were retained. We then removed any gene functionally annotated with 'transpos*'
189 (transposon, transposase, etc.), 'ribonuclease H,' 'pol poly,' 'mitochondri*,' 'chloroplast,' or 'retrovirus.'
190 This filtered annotation contained 30,641 genes.

192 **Differential expression and SNP calling**

193 We performed differential expression analyses using DESeq2 (v. 1.28.1) [49] and our new annotation.
194 For DESeq2 analyses, we aligned reads to the new genome pseudomolecules using STAR version 2.7.6a
195 [49] and generated readcounts using featureCounts (2.02) [50]. Cutoffs for differential expression were
196 as follows: adjusted p-value <0.1, absolute Log2Fold change >1. We identified genes that were
197 differentially expressed between male and female leaf tissues using published leaf RNA sequence data
198 from population samples of the XY cytotype [17], and between male and female floral tissue using
199 published RNA sequence data from the XY cytotype [21]. Genes with fewer than 20 reads across all
200 samples were removed from these analyses. We also identified sequences that were differentially
201 expressed in pollen tissue compared to male leaf tissue, using published sequence data [21]. Finally, we
202 identified sequences differentially expressed in pollen tubes compared to pollen, using pollen from the
203 individuals in the mapping population described [18]. We collected pollen using a kief box (Wacky
204 Willy's, Victoria, BC, Canada), germinated and grew it in 100 μ L of media [51] for 24 hours, and flash
205 froze it in LN2. After removing media, we lysed cells and extracted total RNA using Spectrum Plant Total
206 RNA Kits (Sigma Aldrich) for RNA extraction. To identify sex-linked SNPs and fixed differences between
207 the X and Y chromosome (all females homozygous reference or non-reference, all males heterozygous)
208 for our new assembly, we used FreeBayes v0.9.10-3-g47a713e [52] to call SNPs from the population
209 transcriptome data from the XY cytotype (six males and six females) [17] and the crossing transcriptome
210 data from the same cytotype (six male and six female offspring, plus parents) [17]. We filtered the SNPs
211 to exclude any with a SNP quality score of lower than 60, any sites with missing data, and fixed
212 heterozygous SNPs across all samples that likely reflected paralogous mapping.

213

214 **Linear modelling predictors of recombination rate**

215 We combined our linkage map data with our annotation, TE annotation, differential expression data and
216 summed and averaged variables in 1-Mb windows to perform analyses of recombination landscape,
217 gene content, and differential expression in R version 4.1.0 [53] in RStudio version 1.4.1717 [54] using
218 the packages dplyr version 1.0.7 [55] and stringr version 1.4 [56]. We performed correlations using R's
219 built-in cor function, and estimated partial correlations using the package ppcor version 1.1 [57].

220

221 To identify factors associated with genome structure that predicted recombination rates and
222 recombination rate differences [58], we created linear models with the following response variables:
223 female crossovers per window, male crossovers per window, sex-averaged crossovers per window,
224 crossover number sex difference per window, and female vs. male biased recombination across window.
225 We fit all responses using generalized linear models with either negative binomial or Tweedie
226 distributions except for female versus male biased recombination, for which we used logistic regression.
227 We performed linear models in glimmTMB version 1.12 [59], evaluated fit using DHARMA version 0.4.3
228 [60], and compared models using ANOVAs. We performed separate models for each response variable
229 on each chromosome. Scripts are available at <https://github.com/joannarifkin/Rumex-sex-specific>.

230

231 **Results**

232 **Linkage mapping and genome assembly improvement**

233 We identified five linkage groups, consistent with both the karyotype of the XY cytotype of this species
234 [16, 61] and our previous sex-averaged linkage mapping results [18] (table 1). We again identified two
235 apparently metacentric linkage groups (A1 and A2) and three apparently submetacentric linkage groups
236 (A3, A4, XY) based on the patterns of recombination across the chromosomes (figure 1A) and the
237 identities of the scaffolds constituting the linkage groups. We have retained the same autosomal labels
238 across both maps, and they continue to reflect chromosome sizes from largest (A1) to smallest (A4).

239

240 Our larger genetic mapping population and improved genome assembly led to considerable
241 improvement in higher-order chromosome-scale scaffolding of the genome of *R. hastatulus*. Our
242 improved genome assembly contained 1.45Gb, a reduction of 0.2Gb from our previous 1.65Gb assembly
243 [18] due to the collapsing of redundant haplotypes (see Methods). For this assembly, 1.212Gb (84%) is
244 now grouped in the five linkage groups (previously 1.08GB, 65% of the previous primary assembly), with
245 the remaining 0.23Gb in smaller contigs. These corrections have substantially increased the size of the
246 assembled sex chromosome, with an additional 88.6 MB of sequence assembled on the sex
247 chromosome, the largest increase of any of the chromosomal scaffolds (table 1). Consistent with this
248 increase, analysis of our past genome assembly showed that only 52% of sex-linked SNPs mapped to the
249 assembled sex chromosome; our new assembly integrated with transcriptomes from independent
250 crossing data [17] now shows that 94% of SNPs showing X-Y segregation patterns map to the sex
251 chromosome.

252 **Recombination rates**

253 As in our previous study, we found that recombination was unevenly distributed across the genome,
254 with very large non-recombining regions on all chromosomes (figure 1). We identified clear evidence of
255 heterochiasmy (table 1, figure 1A). Male map lengths were shorter than female map lengths: across
256 chromosomes, female map length was 1.4x male map length (table 1, figure 1A), and the sex
257 chromosome was not an obvious outlier for this metric. Males also had longer blocks of non-
258 recombining windows across all chromosomes. To summarize this pattern, we identified the longest
259 stretches of markers on each chromosome with zero crossovers. On the autosomes, males had runs of
260 non-recombining windows approximately twice as long as those of females, with male-specific non-
261 recombining regions as large as 238MB (table 1). By this measure, the sex chromosomes were an
262 exception: the largest run of male-specific non-recombining windows on the sex chromosome was four
263 times the length of the longest run of female-specific non-recombining sequence (table 1). Thus,
264 although all chromosomes exhibited reduced male recombination rates, the XY chromosome showed
265 the largest region of differentially suppressed recombination between the sexes despite not being the
266 largest chromosome. Overall, male and female recombination rates in *R. hastatulus* were only weakly
267 correlated ($r=0.333$, correlation of male and female crossover number across 1Mb windows across all
268 chromosomes; figure 2, table S1).

270 The extent of sex differences in recombination varied both along and between chromosomes (figure
 271 1B). Chromosomes A1, A2, and the sex chromosome conformed to the common pattern of more tip-
 272 focused recombination in males, but the submetacentric chromosome A3 showed female-biased
 273 recombination in the more highly recombining end, and A4 appeared to have low-recombination
 274 regions at both ends. This differs from the previous linkage map, likely because of the difficulty of
 275 positioning low-recombination regions. In general, pericentromeric regions showed reduced
 276 recombination in both sexes, but female map lengths were larger in these regions and showed apparent
 277 hotspots of recombination with large jumps in centimorgan position (figure 1). All five chromosomes
 278 had regions of female-biased and male-biased recombination, as well as shared recombining and non-
 279 recombining regions (figure 1B). This complex pattern creates a highly heterogeneous recombination
 280 landscape.

281

282

283

284

| LG | Sex-averaged map length(cM) | Male map length (cM) | Female map length (cM) | Mb* | Number of genes | Largest size of markers with 0 crossover events (Mb), in males/females |
|----|-----------------------------|----------------------|------------------------|-------------------|-----------------|--|
| A1 | 104.57 | 94.624 | 114.516 | 388.3386 (344.5) | 7512 | 238.6 / 94.3 |
| A2 | 91.67 | 79.032 | 104.301 | 278.2766 (260.43) | 7301 | 33.4 / 22.9 |
| A3 | 69.09 | 48.387 | 89.785 | 171.7219 (175.01) | 3923 | 91.5 / 44.3 |
| A4 | 61.29 | 52.688 | 69.892 | 135.2128 (158.24) | 3502 | 62.4 / 30.2 |
| XY | 79.03 | 64.516 | 93.548 | 239.0056 (150.39) | 4752 | 212.1 / 55.3 |

*Values in brackets indicate the lengths from the previous assembly

285 **Gene and TE content**

286 As in our previous study, we found that genes were generally concentrated in high-recombination
287 regions (figure 1D). However, A1 contained one gene-dense yet low-recombination region (~100Mb-
288 200Mb). RNA (class 1) TEs were concentrated in low-recombination regions, whereas DNA (class 2) TEs
289 were concentrated in high-recombination regions (figure 1E). Despite the reduced gene density in low-
290 recombination regions, the extent of high recombination-suppressed regions means that a large fraction
291 of genes in the genome (approximately 37%) are in these large regions with no male recombination.
292 Ribosomal genes were concentrated mostly on A3 (62 rDNA features annotated) and A4 (28 rDNA
293 features annotated). rDNA genes occurred in the first 50Mb of A3 (5S subunit sequence) with additional
294 rDNA sequence located around 130Mb of A3 (18S and 28S subunit sequence) and in the first 3 Mb of A4
295 (18S and 28S subunit sequence). These rDNA locations are consistent with past cytological findings [61],
296 further confirming our identification of the A3 and A4 chromosomes.

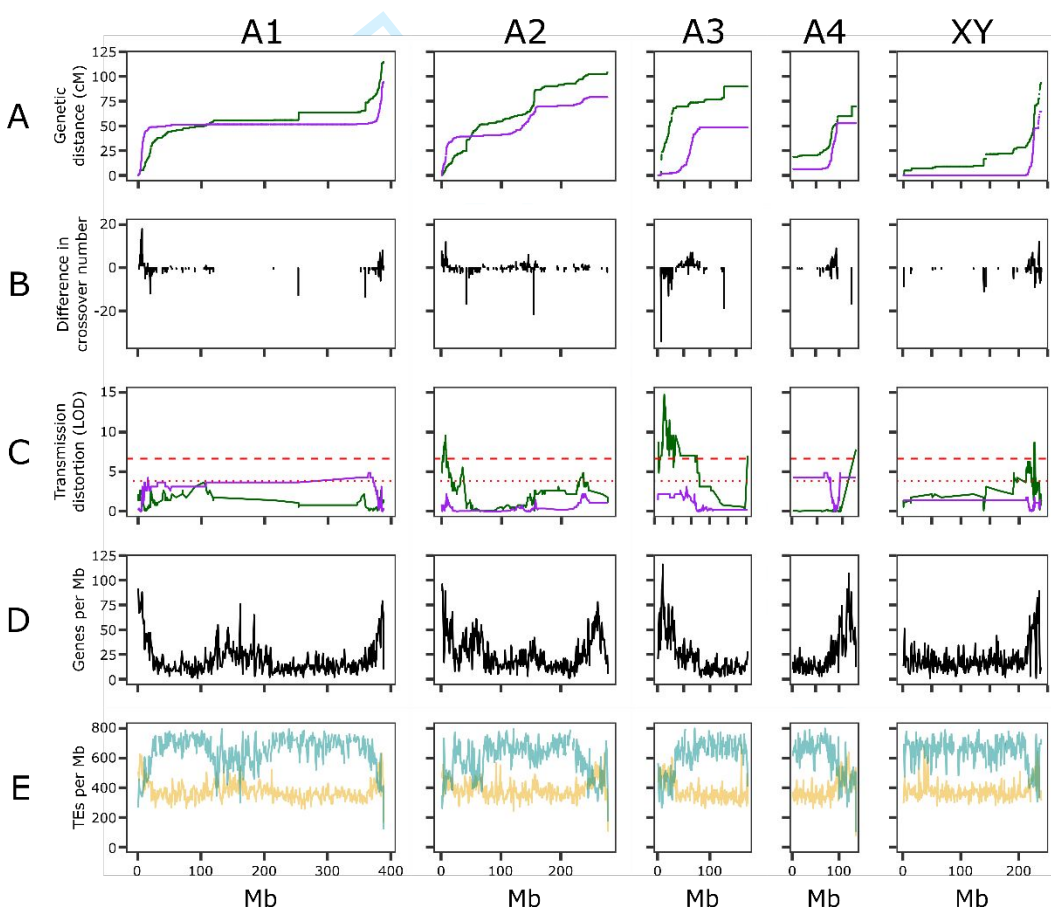
298 **Characterization of the sex-determining (SDR) and pseudo-autosomal regions**

299 With female and male recombination separated, it is clear that the male-specific non-recombining
300 region on the sex chromosome in *R. hastatulus*, i.e. the SDR, is extensive. In particular, our linkage
301 mapping suggests that the SDR is as large as 209MB (14% of the total assembly: table 1, figure 1),
302 including as many as 3595 genes (12% of the total filtered annotated genes). The gene-dense
303 recombining pseudoautosomal region of the sex chromosome is similarly the smallest male recombining
304 segment of any chromosome, representing only approximately 13% of the physical size of the
305 chromosome. Note that the 'true' SDR may be narrower and the pseudoautosomal region larger, since
306 rare male recombination may have gone unobserved in our cross. However, BLAST [37] searches of our
307 sex-linked transcripts that have at least one fixed difference between the X and Y chromosomes from a
308 population sample [17] are found across most of the length of this nonrecombining region (from 1.6 MB
309 to 208.5 MB), and fixed differences mapped onto the chromosome are common across the first 210 MB
310 (figure S1) suggesting that most of this region is nonrecombining and linked to the SDR.

311 **Transmission ratio distortion**

312 We identified loci with biased haplotype transmission through either paternal or maternal inheritance
313 based on the haplotype reconstructions from Lep-Map 3. Transmission ratio distortion varied between

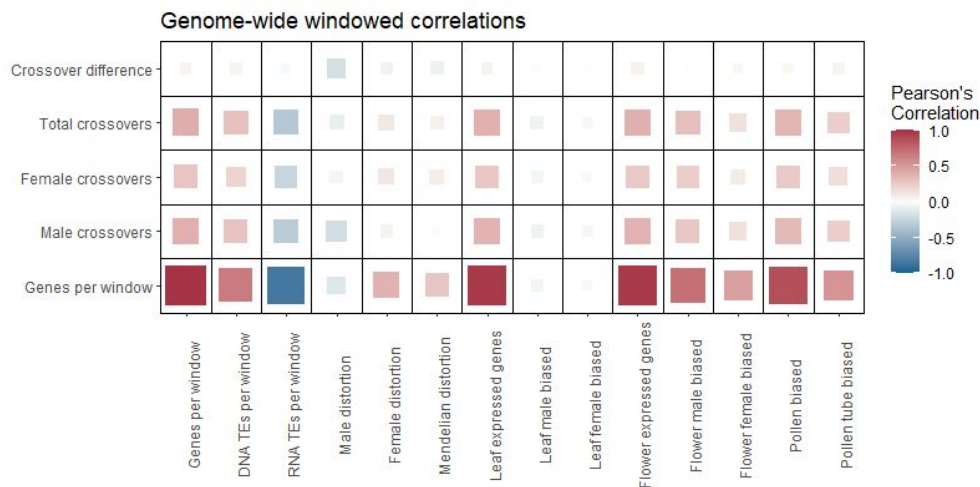
1
2
3 314 chromosomes (figure 1C, figure S2, table S2). More sites experienced biased transmission through
4 315 maternal (276) than paternal (48) inheritance, across a larger fraction of the genome. On A1, 18 sites
5 316 were significantly distorted in transmission from males using a 0.05 cutoff in a chi-squared distribution
6 317 (LOD > 3.841) and on A4, 30 sites were significantly distorted in transmission from males with a 0.05
7 318 cutoff. Although deviations from 1:1 male haplotype transmission occurred on other chromosomes,
8 319 there were no significant male-distorted sites on A2, A3, or the sex chromosome. In contrast, female
9 320 haplotype distortion was extensive on A2 (91 sites in females at 0.05, 38 at 0.01 cutoff of LOD > 6.635),
10 321 A3 (108 sites at .05 cutoff, 88 at 0.01), and the sex chromosome (76 sites at a 0.05 cutoff, 26 at 0.01) but
11 322 negligible on A1 (0 sites) and A4 (1 site at 0.01).



323
324 Figure 1. Distribution of recombination, segregation distortion, and gene content in *Rumex hastatulus*. A. Male
325 (purple) and female (green) Marey maps of the chromosomes. B. Difference in crossover number for 1Mb
326 windows along the chromosome (male crossovers per window - female crossovers per window). Positive: male
327 crossover excess. Negative: female crossover excess. C. Segregation distortion for male (purple) and female (green)
328 haplotypes. Dashed red lines indicate significance at 0.05 and 0.01 levels according to a chi-squared test. D. Genes
329 per 1Mb window along the genome. E. TEs per 1Mb window along the genome. Yellow: DNA TEs. Blue: RNA TEs.
330
331
332

331 Correlates of recombination rate differences

332 Across the genome, the number of genes, leaf- and flower-expressed genes, and DNA (Class 2) TE
 333 density were all positively correlated with recombination rate, and RNA (Class 1) TE density was
 334 negatively correlated with recombination rate (figure 2, table S1, figure S3-S6). Male crossover number
 335 and female crossover number were both positively correlated with gene density, but this correlation
 336 was stronger for male crossovers (male Pearson's $r=0.390$, female Pearson's $r=0.278$). However, the
 337 correlations between transmission ratio distortion and crossover number were in opposite directions: in
 338 females, more distorted regions were also more recombining ($r=0.111$) whereas in males distortion was
 339 negatively correlated with crossover number ($r=-0.197$), reflecting the fact that male transmission
 340 distortion signals were enriched in the large non-recombining regions of male meiosis (figure 1).
 341 Correlations varied in strength between chromosomes, with notable differences in correlates of
 342 transmission ratio distortion and recombination rate difference, both of which varied in magnitude,
 343 position, and direction along and between chromosomes (figure 2, figure S7, table S3). The difference in
 344 crossover number between the sexes was most strongly correlated with signals of male distortion
 345 (figure 2), where regions of particularly low male crossover number represented regions with larger
 346 signals of male distortion. We also estimated partial correlation coefficients controlling for gene density,
 347 which was consistently correlated with many genomic variables (figure S8, figure S9, tables S4-S5).
 348 Correlations between distortion and crossover number in both males and females persisted after
 349 controlling for gene density, and varied in direction across chromosomes (figure S9). However, all
 350 chromosomes except A2 showed a consistent negative correlation between male-biased recombination
 351 and male transmission distortion, even when gene density was controlled.



354 Figure 2: Correlations among genome window characteristics across the whole genome of *Rumex hastatulus*.
355 Colours and sizes correspond to the strength and direction of the correlations.
356

357 Linear models of recombination rate differences

358 We used generalized linear models to identify predictors of sex-specific and sex-averaged recombination
359 rates, whether recombination was male- or female-biased, and the magnitude of the recombination rate
360 difference in *R. hastatulus*. Full modeling results are available in table S6 and table S7.

361
362 In our linear models, the variables that significantly predicted male recombination rate varied between
363 chromosomes (table 2A). Number of genes predicted increased male recombination rate on three
364 chromosomes (as well as a fourth in some models), and position along the genome emerged as an
365 important predictor on two submetacentric chromosomes, suggesting that distance from centromere
366 predicts male recombination (figure 1). RNA TE count also appeared to play a role, but in inconsistent
367 directions, predicting increased male recombination on two chromosomes and decreased male
368 recombination on a third; this pattern also appears in the partial correlations with gene density removed
369 (figure S9). Transmission ratio distortion predicted reduced male recombination rate on three
370 chromosomes (A2, A3, and A4), and predicted increased male recombination on A1. Either pollen bias or
371 pollen tube bias predicted male recombination rate on three chromosomes (negatively on A4 and the
372 sex chromosome, positively on A3).

373
374 In contrast, the predictors of female recombination are more consistent across chromosomes (table 2B).
375 Number of genes per window positively predicted female recombination rate on all five chromosomes,
376 and position relative to centromere affected female recombination rate on four chromosomes. Only one
377 other variable, pollen tube-biased expression, predicted female recombination rate on more than one
378 other chromosome. Female transmission ratio distortion did not emerge as a significant predictor of
379 recombination rate on any chromosome.

380
381 Predictors of both sex-averaged recombination and of the magnitude of the recombination rate
382 difference between males and females reflected predictors of male and female recombination rate
383 independently. Number of genes, position along the chromosome, number of RNA TEs, female-biased
384 floral expression, pollen tube-biased expression all appeared as significant predictors, but their
385 importance and direction varied between chromosomes (table S6A, S6B).

386
 387 Finally, we used logistic regression to identify variables that predicted whether windows exhibited
 388 female or male recombination bias (table S6C). Our logistic regressions also suggested considerable
 389 variation in the factors that predicted sex differences in recombination. Number of genes per window
 390 was an important predictor for four out of five chromosomes, but in variable directions, predicting both
 391 male bias (A1, XY) and female bias (A2, A3) in recombination.

Table 2

Variables identified as significant predictors of recombination in linear models of windows of the *Rumex hastatulus* genome.

Male recombination rate predictors

'+' - variable predicts increased male recombination. '-' - variable predicts decreased male recombination. * - 95% confidence interval for slope estimate includes zero, chiefly because term is significant in interaction term.

| | # genes | Position | # RNA TEs | Male distortion | Pollen tube bias | Pollen bias |
|----------|---------|----------|-----------|-----------------|------------------|-------------|
| A1 | + | | + | + | | |
| A2 | + | | +* | -* | | |
| A3 (neo) | ~ +* | -* | | -* | + | |
| A4 | | | - | - | - | |
| XY | +* | + | | | | - |

Interaction effects in best model:

A1: n RNA TEs:male distortion (-)

A2: n genes:male distortion (+ ns)

A3: male distortion:position window (+)

A3 (more complex model): position window:n genes (- ns), male distortion:position window (+), n genes:male distortion, n genes:position window:male distortion (+ns)

A4: none

XY: position window:n genes (-)

Female recombination rate predictors

'+' - variable predicts increased female recombination. '-' - variable predicts decreased female recombination. * - 95% confidence interval for slope estimate includes zero, chiefly because term is significant in interaction term.

| | # genes | Position | # RNA TEs | Flower female bias | Pollen tube bias | Leaf expression |
|----------|---------|----------|-----------|--------------------|------------------|-----------------|
| A1 | +* | | _* | | - | |
| A2 | +* | _* | | | | |
| A3 (neo) | + | _* | | | | - |
| A4 | + | + | | | | |
| XY | +* | + | | + | +* | |

418

419 Interaction effects in best model:

420

420 A1: n RNA TEs:pollen tube bias (+)

421

421 A2: n genes: position window (-ns)

422

422 A3: n genes: position window (-), leaf expression: position window (+)

423

423 A4: n genes: position window (- ns)

424

424 XY: position window:female flower bias (-)

425

425 XY (more complex model): position window:female flower bias (-), position window:pollen tube bias (-

426

426 ns), position window:pollen tube bias:flower female bias (+)

427

428

428 Discussion

429

429 The main findings of this study are consistent with the general pattern of extensive recombination

430

430 suppression that we previously inferred based on sex-averaged recombination in *R. hastatulus* [18].

431

431 However, our sex-specific maps show that recombination suppression is not evenly distributed between

432

432 males and females, and that the observed very large pericentromeric regions of suppressed

433

433 recombination are particularly influenced by highly suppressed male recombination. Across all

434

434 chromosomes, females recombine more frequently than males and males have much larger non-

435

435 recombining blocks than females. Our results are in line with several studies of hermaphroditic plants, as

436

436 well as other eukaryotes [1], with the very large male-specific non-recombining regions that we report

437

437 making this an extreme case.

438

439

439 However, *R. hastatulus* does not strictly follow the common eukaryotic pattern of tip-focused male

440

440 recombination [1] across all chromosomes. The recombination landscapes of both the metacentric and

441

441 submetacentric chromosomes suggest greater variation in the distribution of recombination than simply

442

442 less male recombination in the centres and more at the chromosome ends, with highly recombining

443

443 regions scattered along chromosomes (particularly A2, A3, and A4). Thus, male recombination is more

444

444 concentrated, but not always at the tips of the chromosome. These differences among chromosomes

445

446

447

448

449

450

451

1
2
3 445 may reflect an ongoing history of chromosomal rearrangements in the genus and additional patterns of
4 446 chromosome structure such as the locations of centromeres and rDNA clusters [61].

5
6 447
7
8 448 The pattern of larger non-recombining regions in males is consistent with an evolutionary bias toward
9 449 the evolution of male heterogamety and XY sex chromosomes in *Rumex*. In particular, suppressed
10 450 recombination can facilitate the maintenance and invasion of sexually antagonistic variants linked to
11 451 sex-determining regions [62], and sex-determining regions that evolve in large pericentromeric non-
12 452 recombining regions, especially sex-specific ones, may contribute to the evolution of sex chromosomes
13 453 [63]. The existence of male-specific non-recombining regions may thus facilitate the evolution of XY
14 454 rather than ZW sex chromosomes [1]. Given our observation of no crossovers in male meiosis over very
15 455 large fractions of each chromosome, it is possible that recombination suppression was ancestral to the
16 456 evolution of dioecy in the genus, and that subsequent recombination modifiers did not evolve following
17 457 the origin of the SDR. The observed size of the SDR, which is over 200 MB using population-validated
18 458 sex-linked genes and includes over 14% of the assembled genome and over 3500 genes, is much larger
19 459 than those recently reviewed to date in plants [64], although larger population samples of *R. hastatulus*
20 460 should be used to test for very rare recombination between the X and Y, and the sex-linked region of *S.*
21 461 *latifolia* may be even larger [65]. Although we cannot rule out a role for subsequent recombination
22 462 modifiers, particularly because the sex chromosomes show the most extreme size dimorphism of the
23 463 nonrecombining region (table 1), our results do suggest that sex differences in heterochiasmy may have
24 464 played an important role in determining the large size of the SDR facilitating the evolution of large
25 465 heteromorphic sex chromosomes in this system. Comparative studies of heterochiasmy in both
26 466 hermaphroditic and other dioecious species in *Rumex* will be important to further assess the extent to
27 467 which ancestral heterochiasmy and derived changes in recombination rates have contributed to sex
28 468 chromosome evolution in this lineage.

29
30
31
32
33
34
35 469
36 470 Models for the evolution of heterochiasmy due to male haploid selection and female meiotic drive both
37 471 predict lower overall male recombination rates and higher female recombination near centromeres
38 472 [1,6,7], as we observed in *R. hastatulus*. Our mapping population provided evidence for both male and
39 473 female transmission ratio distortion, which varied within and among chromosomes and between the
40 474 sexes. Overall, more sites displayed significant distortion in female than in male transmission, but
41 475 significant regions of both types of distortion were observed across the genome. Transmission ratio
42 476 distortion through female inheritance is generally thought to be consistent with female meiotic drive. In

1
2
3 477 contrast, transmission ratio distortion through male inheritance may result from haploid (pollen)
4 478 competition [66].

5 479
6
7
8 480 Nevertheless, zygotic distortion (i.e., differential seed germination or seedling survival) could also lead
9 481 to transmission ratio distortion, and may result from alleles inherited from either parent [66].

10 482 In our study, we genotyped reproductive adults rather than pollen or seeds, which conflates several
11 483 opportunities for natural and sexual selection causing biased transmission. Zygotic selection may be
12 484 particularly likely to explain our observed female distortion, since these regions were not focused on
13 485 low-recombination centromeric regions, where meiotic drive is expected to act [7]. In contrast, signals
14 486 of male transmission distortion are particularly enriched in regions of low male recombination and high
15 487 sex bias in recombination (figure 1 and figure 2, table 2), suggesting that haploid selection in males may
16 488 be an important selective pressure for sex differences in recombination. Distorted regions can vary
17 489 widely between populations of the same species [67], so distortion in a single cross should be
18 490 interpreted with some caution. Furthermore, patterns of biased pollen or pollen tube expression do not
19 491 show similarly consistent enrichment in regions of low male recombination except for the sex
20 492 chromosome (table 2, figure S6), although direct observation of transmission distortion likely provides a
21 493 stronger indicator of loci involved in pollen competition. Similarly, although we did not identify evidence
22 494 consistent with ongoing recombination increases to counter meiotic drive, the overall pattern of
23 495 increased and more centromere-biased recombination is still consistent with a history of selection
24 496 eliminating meiotic drive alleles. With those caveats, our results do provide some evidence in accord
25 497 with the hypothesis that pollen competition may play an important role in sex differences in
26 498 recombination.

27 499
28
29
30 500 We used both pairwise correlations and regression models to investigate various genomic correlates of
31 501 male and female recombination and sex bias in recombination, in order to further explore other possible
32 502 factors favouring sex differences in recombination. On a genome-wide scale, both male and female
33 503 recombination rates in *R. hastatulus* are consistent with widely observed patterns that genes and Class 2
34 504 DNA TEs concentrate in high-recombination regions and Class 1 RNA TEs concentrate in low-
35 505 recombination regions (figure 2; [3], [56]). These patterns are consistent with recombination rates in
36 506 plants occurring preferentially upstream of genes, and with epigenetic silencing of retrotransposable
37 507 elements causing a reduction of recombination, although they could also be explained if transposable
38 508 elements preferentially accumulate in regions of low sex-averaged recombination [3].

509
510 Because the recombination landscape varied widely between the chromosomes of *R. hastatulus*, we
511 also identified chromosome-specific predictors of recombination rates and recombination rate bias
512 using linear models and partial correlations controlling for gene density. At this more granular scale, a
513 different and more complex picture emerges (table 2, figure S8, S9). In particular, our logistic regression
514 models of recombination bias direction support the possibility that different mechanisms may be
515 contributing to variation in recombination rates on different chromosomes. Both number of genes per
516 window and position along the genome predicted female-biased recombination on some chromosomes
517 and male-biased recombination on others. Aside from physical position and gene density, different
518 diverse factors predicted both male and female bias on different chromosomes, including RNA TEs,
519 number of genes expressed in different tissues, sex-biased floral expression, pollen-biased expression,
520 and transmission ratio distortion (table 2C). This finding suggests a general picture in which gene density
521 and proximity to centromere shape recombination on a 'global scale', but variation in gene content and
522 haploid selection may lead to region-specific selective forces acting on both male and female
523 recombination rates. Consistent with this, a recent comparative study in fish [68] found that sex
524 differences in recombination are labile at the species level, but do not present clear trends consistent
525 with adaptive hypotheses across species.

526
527

528 Conclusions

529 Our study has provided some of the first evidence of sex differences in recombination and identified one
530 of the largest known SDRs in a dioecious plant species, or in fact in any eukaryote [65]. We identified
531 both genome-wide and chromosome-specific factors predicting sex differences in recombination, and
532 also found evidence consistent with a role for male gametophytic selection in driving these differences.
533 Future work in this system will allow more precise dissection of the genetic and evolutionary
534 mechanisms favouring sex differences in recombination landscapes. In particular, exploring both sex-
535 specific eQTL positions and further study of transmission ratios in pollen and seeds will allow us to
536 further differentiate between sexually antagonistic cis epistasis in diploids and epistasis in haploids [1].
537 Finally, characterizing sex-specific recombination landscapes of hermaphroditic *Rumex* species should
538 make it possible to determine whether these sex differences in recombination landscape did indeed

1
2
3 539 precede and promote the evolution of a heterogametic XY sex determining system with a very large
4
5 540 SDR, as we have hypothesized.

6 541

10 542 Acknowledgments

11
12 543 We thank University of Toronto undergraduate students Victoria Marshall, Claire Ellis, Deanna Kim, and
13
14 544 Madeline Jarvis-Cross for technical assistance, Bill Cole and Tom Gludovac for glasshouse support, and
15
16 545 Brechann McGoey for crossing chamber development. This research was supported by Discovery grants
17
18 546 from the Natural Sciences and Engineering Research Council of Canada to SCHB and SIW. JLR was
19
20 547 supported by an EEB post-doctoral fellowship.

23 548 Data accessibility statement

24
25 549 Raw sequence has been deposited on the Sequence Read Archive (SRA) under the accession number
26
27 550 PRJNA692236 (embargoed until July 1, 2022 or publication). Our new genome assembly, transcriptome
28
29 551 annotation, rDNA annotation, and TE annotation have been deposited in the CoGe comparative
30
31 552 genomics platform at <https://genomevolution.org/coge/GenomeInfo.pl?gid=62326>. Scripts used in the
32
33 553 analyses have been deposited on Github at <https://github.com/joannarifkin/Rumex-sex-specific>.

34 554

35 555

36 556

39 557 References

40
41 558

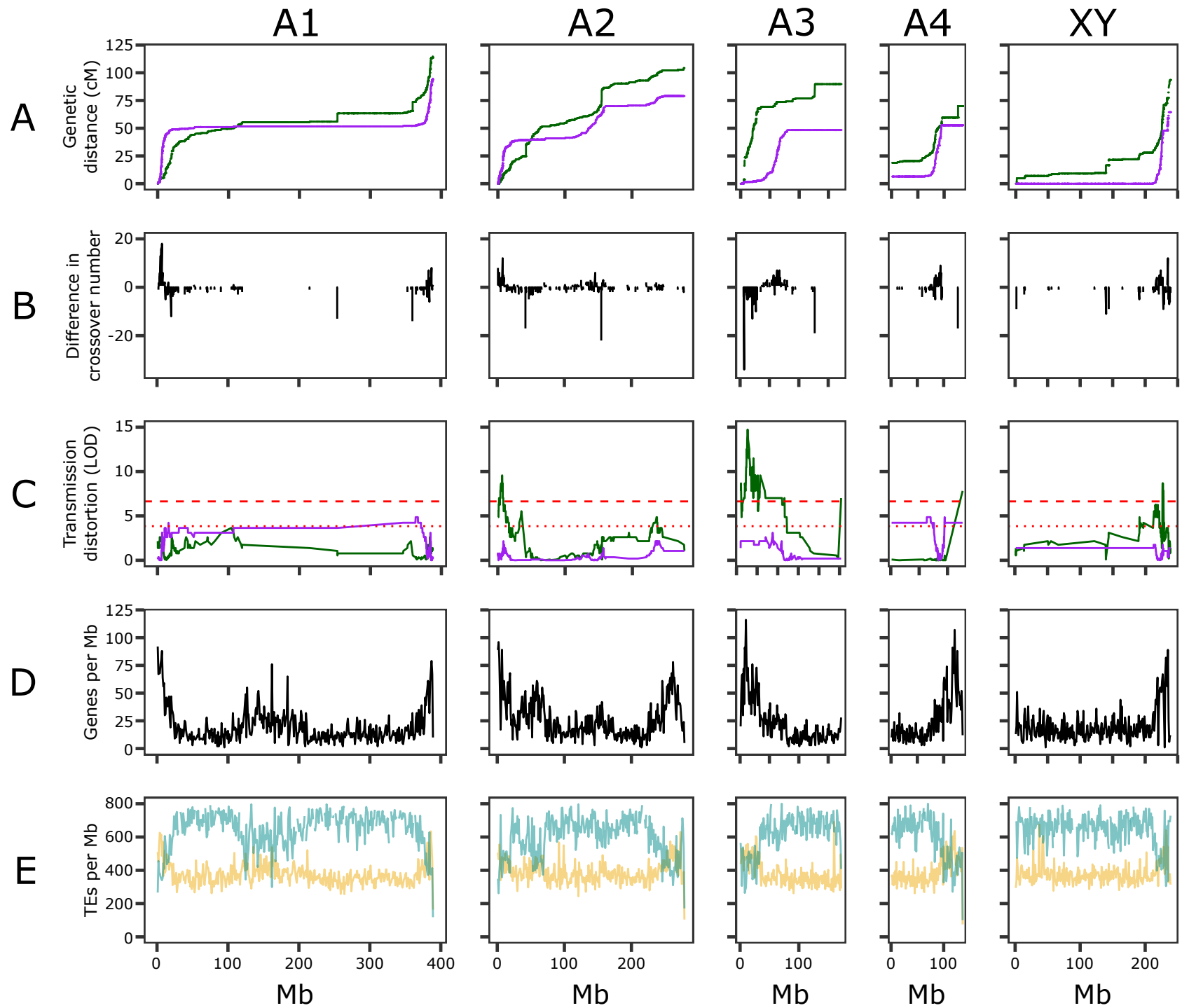
- 43 559 1. Sardell JM, Kirkpatrick M. 2020 Sex differences in the recombination landscape. *Am. Nat.* **195**,
44 560 361–379.
- 45 561 2. Campos JL, Halligan DL, Haddrill PR, Charlesworth B. 2014 The relation between recombination
46 562 rate and patterns of molecular evolution and variation in *Drosophila melanogaster*. *Mol. Biol.*
47 563 *Evol.* **31**, 1010–1028.
- 49 564 3. Kent TV, Uzunović J, Wright SI. 2017 Coevolution between transposable elements and
50 565 recombination. *Philos. Trans. R. Soc. Lond. B Biol. Sci.* **372**, 20160458.
- 51 566 4. Nachman MW, Payseur BA. 2012 Recombination rate variation and speciation: theoretical
52 567 predictions and empirical results from rabbits and mice. *Philos. Trans. R. Soc. Lond. B Biol. Sci.*
53 568 **367**, 409–421.
- 54 569 5. Stapley J, Feulner PGD, Johnston SE, Santure AW, Smadja CM. 2017 Variation in recombination
55 570 frequency and distribution across eukaryotes: patterns and processes. *Philos. Trans. R. Soc.*

- 1
2
3 571 *Lond. B Biol. Sci.* **372**, 20160455.
- 4 572 6. Lenormand T, Dutheil J. 2005 Recombination difference between sexes: a role for haploid
5 573 selection. *PLoS Biol.* **3**, e63.
- 6 574 7. Brandvain Y, Coop G. 2012 Scrambling eggs: meiotic drive and the evolution of female
7 575 recombination rates. *Genetics* **190**, 709–723.
- 8 576 8. Johnston SE, Huisman J, Ellis PA, Pemberton JM. 2017 A high-density linkage map reveals sexual
9 577 dimorphism in recombination landscapes in Red Deer (*Cervus elaphus*). *G3* **7**, 2859–2870.
- 10 578 9. Bergero R, Gardner J, Bader B, Yong L, Charlesworth D. 2019 Exaggerated heterochiasmy in a
11 579 fish with sex-linked male coloration polymorphisms. *Proc. Natl. Acad. Sci. U. S. A.* **116**, 6924–
12 580 6931.
- 13 581 10. Giraut L, Falque M, Drouaud J, Pereira L, Martin OC, Mézard C. 2011 Genome-wide crossover
14 582 distribution in *Arabidopsis thaliana* meiosis reveals sex-specific patterns along chromosomes.
15 583 *PLoS Genet.* **7**, e1002354.
- 16 584 11. Lagercrantz U, Lydiate DJ. 1995 RFLP mapping in *Brassica nigra* indicates differing recombination
17 585 rates in male and female meioses. *Genome.* **38**, 255–264.
- 18 586 12. Phillips D *et al.* 2015 The effect of temperature on the male and female recombination
19 587 landscape of barley. *New Phytol.* **208**, 421–429.
- 20 588 13. Kianian PMA *et al.* 2018 High-resolution crossover mapping reveals similarities and differences
21 589 of male and female recombination in maize. *Nat. Commun.* **9**, 2370.
- 22 590 14. de Vicente MC, Tanksley SD. 1991 Genome-wide reduction in recombination of backcross
23 591 progeny derived from male versus female gametes in an interspecific cross of tomato. *Theor.*
24 592 *Appl. Genet.* **83**, 173–178.
- 25 593 15. Veltsos P *et al.* 2019 Early sex-chromosome evolution in the diploid dioecious plant *Mercurialis*
26 594 *annua*. *Genetics* **212**, 815–835.
- 27 595 16. Smith BW. 1964 The evolving karyotype of *Rumex hastatulus*. *Evolution* **18**, 93–104.
- 28 596 17. Hough J, Hollister JD, Wang W, Barrett SCH, Wright SI. 2014 Genetic degeneration of old and
29 597 young Y chromosomes in the flowering plant *Rumex hastatulus*. *Proc. Natl Acad. Sci. USA* **111**,
30 598 7713–7718.
- 31 599 18. Rifkin JL, Beaudry FEG, Humphries Z, Choudhury BI, Barrett SCH, Wright SI. 2021 Widespread
32 600 recombination suppression facilitates plant sex chromosome evolution. *Mol. Biol. Evol.* **38**,
33 601 1018–1030.
- 34 602 19. Field DL, Pickup M, Barrett SCH. 2012 The influence of pollination intensity on fertilization
35 603 success, progeny sex ratio, and fitness in a wind-pollinated, dioecious plant. *Int. J. Plant Sci.* **173**,
36 604 184–191.
- 37 605 20. Pickup M, Barrett SCH. 2013 The influence of demography and local mating environment on sex
38 606 ratios in a wind-pollinated dioecious plant. *Ecol. Evol.* **3**, 629–639.
- 39 607 21. Sandler G, Beaudry FEG, Barrett SCH, Wright SI. 2018 The effects of haploid selection on Y
40 608 chromosome evolution in two closely related dioecious plants. *Evol Lett* **2**, 368–377.
- 41 609 22. Wilby AS, Parker JS. 1988 Mendelian and non-Mendelian inheritance of newly-arisen
42 610 chromosome rearrangements. *Heredity* **60**, 263–268.
- 43 611 23. McGoey BV, Janik R, Stinchcombe JR. 2017 Individual chambers for controlling crosses in
44 612 wind-pollinated plants. *Methods Ecol. Evol.* **8**, 887–891.
- 45 613 24. Dobin A, Davis CA, Schlesinger F, Drenkow J, Zaleski C, Jha S, Batut P, Chaisson M, Gingeras TR.
46 614 2013 STAR: ultrafast universal RNA-seq aligner. *Bioinformatics* **29**, 15–21.
- 47 615 25. Dobin A, Gingeras TR. 2016 Optimizing RNA-Seq Mapping with STAR. *Methods Mol. Biol.* **1415**,
48 616 245–262.
- 49 617 26. Van der Auwera GA, O'Connor BD. 2020 *Genomics in the Cloud: Using Docker, GATK, and WDL in*
50 618 *Terra*. Newton, MA: O'Reilly Media, Inc.

27. Rastas P. 2017 Lep-MAP3: robust linkage mapping even for low-coverage whole genome sequencing data. *Bioinformatics* **33**, 3726–3732.
28. Rastas P. 2020 Lep-Anchor: automated construction of linkage map anchored haploid genomes. *Bioinformatics* **36**, 2359–2364.
29. Huang S *et al.* 2012 HaploMerger: reconstructing allelic relationships for polymorphic diploid genome assemblies. *Genome Res.* **22**, 1581–1588.
30. Morgulis A, Gertz EM, Schäffer AA, Agarwala R. 2006 WindowMasker: window-based masker for sequenced genomes. *Bioinformatics* **22**, 134–141.
31. Li H. 2018 Minimap2: pairwise alignment for nucleotide sequences. *Bioinformatics* **34**, 3094–3100.
32. Plotly Technologies Inc. Collaborative data science. Montréal, QC, 2015. <https://plot.ly>.
33. Haldane JBS. 1919 The combination of linkage values and the calculation of distances. *J. Genet.* **8**, 299–309.
34. Cantarel BL, Korf I, Robb SMC, Parra G, Ross E, Moore B, Holt C, Sánchez Alvarado A, Yandell M. 2008 MAKER: an easy-to-use annotation pipeline designed for emerging model organism genomes. *Genome Res.* **18**, 188–196.
35. Peng Y, Leung HCM, Yiu S-M, Lv M-J, Zhu X-G, Chin FYL. 2013 IDBA-tran: a more robust de novo de Bruijn graph assembler for transcriptomes with uneven expression levels. *Bioinformatics* **29**, i326–34.
36. Zhang L *et al.* 2017 The Tartary Buckwheat genome provides insights into rutin biosynthesis and abiotic stress tolerance. *Mol. Plant* **10**, 1224–1237.
37. Altschul SF, Gish W, Miller W, Myers EW, Lipman DJ. 1990 Basic local alignment search tool. *J. Mol. Biol.* **215**, 403–410.
38. Jones P *et al.* 2014 InterProScan 5: genome-scale protein function classification. *Bioinformatics* **30**, 1236–1240.
39. Lagesen K, Hallin P, Rødland EA, Staerfeldt H-H, Rognes T, Ussery DW. 2007 RNAmmer: consistent and rapid annotation of ribosomal RNA genes. *Nucleic Acids Res.* **35**, 3100–3108.
40. Ou S *et al.* 2019 Benchmarking transposable element annotation methods for creation of a streamlined, comprehensive pipeline. *Genome Biol.* **20**, 275.
41. Ou S, Jiang N. 2019 LTR_FINDER_parallel: parallelization of LTR_FINDER enabling rapid identification of long terminal repeat retrotransposons. *Mob. DNA* **10**, 48.
42. Ellinghaus D, Kurtz S, Willhoeft U. 2008 LTRharvest, an efficient and flexible software for de novo detection of LTR retrotransposons. *BMC Bioinformatics* **9**, 18.
43. Ou S, Jiang N. 2018 LTR_retriever: A highly accurate and sensitive program for identification of long terminal repeat retrotransposons. *Plant Physiology.* **176**, 1410–1422.
44. Su W, Gu X, Peterson T. 2019 TIR-Learner, a new ensemble method for TIR transposable element annotation, provides evidence for abundant new transposable elements in the Maize genome. *Mol. Plant* **12**, 447–460.
45. Xiong W, He L, Lai J, Dooner HK, Du C. 2014 HelitronScanner uncovers a large overlooked cache of Helitron transposons in many plant genomes. *Proc. Natl Acad. Sci. USA* **111**, 10263–10268. (doi:10.1073/pnas.1410068111).
46. Flynn JM, Hubley R, Goubert C, Rosen J, Clark AG, Feschotte C, Smit AF. 2020 RepeatModeler2 for automated genomic discovery of transposable element families. *Proc. Natl Acad. Sci. U. S. A.* **117**, 9451–9457.
47. Smit, AFA, Hubley, R & Green, P. 2013-2015 Repeat-Masker Open-4.0. <http://www.repeatmasker.org>. See <https://ci.nii.ac.jp/naid/10029514778/> (accessed on 15 September 2021).
48. Quinlan AR, Hall IM. 2010 BEDTools: a flexible suite of utilities for comparing genomic features.

- 667 *Bioinformatics* **26**, 841–842.
- 668 49. Love MI, Huber W, Anders S. 2014 Moderated estimation of fold change and dispersion for RNA-
669 seq data with DESeq2. *Genome Biol.* **15**, 550.
- 670 50. Liao Y, Smyth GK, Shi W. 2014 featureCounts: an efficient general purpose program for assigning
671 sequence reads to genomic features. *Bioinformatics* **30**, 923–930.
- 672 51. Adhikari KN, Campbell CG. 1998 In vitro germination and viability of buckwheat (*Fagopyrum*
673 *esculentum* Moench) pollen. *Euphytica* **102**, 87–92.
- 674 52. Garrison E, Marth G. 2012 Haplotype-based variant detection from short-read sequencing.
675 *arXiv preprint arXiv:1207.3907.
- 676 53. R Development Core Team. 2021 R: A language and environment for statistical computing. R
677 Foundation for Statistical Computing, Vienna, Austria. See <https://www.R-project.org/>.
678 (accessed on 2021).
- 679 54. R Team. 2020 RStudio: Integrated Development for R. RStudio, PBC, Boston, MA, 2020.
- 680 55. Hadley Wickham RF, Henry L, Müller K. 2017 dplyr: A Grammar of Data Manipulation. R package
681 version 0.7. 4.
- 682 56. Wickham H. 2019 stringr: Simple, consistent wrappers for common string operations. R package
683 version 1.4.0. See <https://CRAN.R-project.org/package=stringr> (accessed on 2019).
- 684 57. Kim, S. (2015) ppcor: An R Package for a fast calculation to semi-partial correlation coefficients.
685 *Commun. Stat. Appl. Methods*, **22(6)**, 665–674.
- 686 58. Paape T, Zhou P, Branca A, Briskine R, Young N, Tiffin P. 2012 Fine-scale population
687 recombination rates, hotspots, and correlates of recombination in the *Medicago truncatula*
688 genome. *Genome Biol. Evol.* **4**, 726–737.
- 689 59. Brooks ME, Kristensen K, Van Benthem KJ, Magnusson A, Berg CW, Nielsen A, Skaug HJ, Machler
690 M, Bolker BM. 2017 glmmTMB balances speed and flexibility among packages for zero-inflated
691 generalized linear mixed modeling. *R J.* **9**, 378–400.
- 692 60. Hartig F. 2019 DHARMA: residual diagnostics for hierarchical (multi-level/mixed) regression
693 models. R package version 0.1. 0.
- 694 61. Kasjaniuk M, Grabowska-Joachimciak A, Joachimciak AJ. 2019 Testing the translocation hypothesis
695 and Haldane’s rule in *Rumex hastatulus*. *Protoplasma* **256**, 237–247.
- 696 62. Otto SP. 2019 Evolutionary potential for genomic islands of sexual divergence on recombining
697 sex chromosomes. *New Phytol.* **224**, 1241–1251.
- 698 63. Charlesworth, D. 2019 Young sex chromosomes in plants and animals. *New Phyt.* **224**, 1095-
699 1107.
- 700 64. Renner SS, Müller NA. 2021 Plant sex chromosomes defy evolutionary models of expanding
701 recombination suppression and genetic degeneration. *Nat Plants* **7**, 392–402.
- 702 65. Gschwend, AR, Weingartner, LA, Moore, RC, and R Ming. 2012 The sex-specific region of sex
703 chromosomes in animals and plants. *Chromosome Res.* **20**, 57–69.
- 704 66. Fishman L, McIntosh M. 2019 Standard Deviations: The biological bases of transmission ratio
705 distortion. *Annu. Rev. Genet.* **53**, 347–372.
- 706 67. Seymour DK, Chae E, Arioiz BI, Koenig D, Weigel D. 2019 Transmission ratio distortion is frequent
707 in *Arabidopsis thaliana* controlled crosses. *Heredity* **122**, 294–304.
- 708 68. Cooney CR, Mank JE, Wright AE. 2021 Constraint and divergence in the evolution of male and
709 female recombination rates in fishes. *Evolution* <https://doi.org/10.1111/evo.14357>

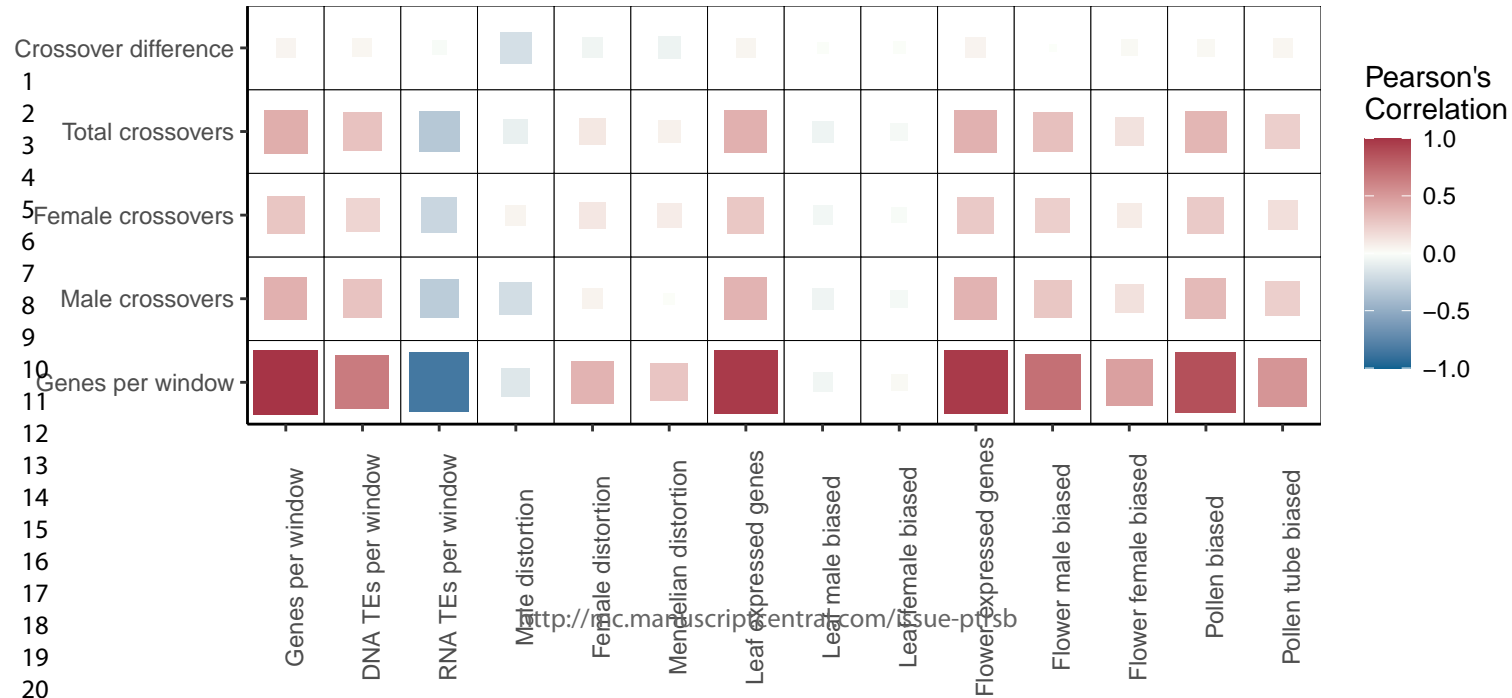
710
711



Genome-wide windowed correlations

Submitted to Phil. Trans. R. Soc. B - Issue

Page 28 of 27



<http://mc.manuscriptcentral.com/issue-psb>